
Article:
Collier, G.J., Schulte, R.F., Rao, M. et al. (2023) Imaging gas-exchange lung function and brain tissue uptake of hyperpolarized 129Xe using sampling density-weighted MRSI. Magnetic Resonance in Medicine, 89 (6). pp. 2217-2226. ISSN: 0740-3194

https://doi.org/10.1002/mrm.29602

Received: 19 July 2022 | Revised: 12 January 2023 | Accepted: 12 January 2023

DOI: 10.1002/mrm.29602

RESEARCH ARTICLE

Magnetic Resonance in Medicine

Imaging gas-exchange lung function and brain tissue uptake of hyperpolarized ^{129}Xe using sampling density-weighted MRSI

Guilhem J. Collier[1,2] | **Rolf F. Schulte**[3] | **Madhwesha Rao**[1] | **Graham Norquay**[1] | **James Ball**[1] | **Jim M. Wild**[1,2]

[1]POLARIS, Imaging Sciences, Department of Infection, Immunity & Cardiovascular Disease, University of Sheffield, Sheffield, UK

[2]INSIGNEO institute, University of Sheffield, Sheffield, UK

[3]GE Healthcare, Munich, Germany

Correspondence
Guilhem J. Collier, MRI unit, University of Sheffield, C Floor, Royal Hallamshire Hospital, Glossop Road, Sheffield, S10 2JF, UK.
Email: g.j.collier@sheffield.ac.uk

Funding information
Medical Research Council, Grant/Award Number: MR/M008894/1

Purpose: Imaging of the different resonances of hyperpolarized ^{129}Xe in the brain and lungs was performed using a 3D sampling density-weighted MRSI technique in healthy volunteers.

Methods: Four volunteers underwent dissolved-phase hyperpolarized ^{129}Xe imaging in the lung with the MRSI technique, which was designed to improve the point-spread function while preserving SNR (1799 phase-encoding steps, 14-s breath hold, 2.1-cm isotropic resolution). A frequency-tailored RF excitation pulse was implemented to reliably excite both the ^{129}Xe gas and dissolved phase (tissue/blood signal) with 0.1° and 10° flip angles, respectively. Images of xenon gas in the lung airspaces and xenon dissolved in lung tissue/blood were used to generate quantitative signal ratio maps. The method was also optimized and used for imaging dissolved resonances of ^{129}Xe in the brain in 2 additional volunteers.

Results: High-quality regional spectra of hyperpolarized ^{129}Xe were achieved in both the lung and the brain. Ratio maps of the different xenon resonances were obtained in the lung with sufficient SNR (> 10) at both 1.5 T and 3 T, making a triple Lorentzian fit possible and enabling the measurement of relaxation times and xenon frequency shifts on a voxel-wise basis. The imaging technique was successfully adapted for brain imaging, resulting in the first demonstration of 3D xenon brain images with a 2-cm isotropic resolution.

Conclusion: Density-weighted MRSI is an SNR and encoding-efficient way to image ^{129}Xe resonances in the lung and the brain, providing a valuable tool to quantify regional spectroscopic information.

KEYWORDS
brain, hyperpolarized ^{129}Xe, lung, spectroscopic imaging

Guilhem J. Collier and Rolf F. Schulte contributed equally to this work.

1 | INTRODUCTION

MRI with hyperpolarized (HP) ^{129}Xe has seen a renewed interest thanks to the development of efficient means of production of large quantities of HP gas,[1–3] the progress in dissolved xenon imaging techniques,[4] and its clinical translation for the measurement of lung gas transfer, which has recently shown promise for assessing the short and long-term effects of coronavirus disease 2019.[5,6] Xenon gas can be safely inhaled, reaching the respiratory airways of the lung where it is absorbed in the alveolar membrane, diffusing into capillaries where it is directly absorbed by the red blood cells. The approximate 8-s T_1 of xenon dissolved in oxygenated blood[7] means that it can also be detected in other well-perfused organs such as the brain and kidneys. Most "dissolved-phase" HP ^{129}Xe applications to date have focused on the lung, where ^{129}Xe exhibits three distinct spectral resonance lines for xenon as gas (0 ppm), dissolved in lung membrane tissue/-plasma (M, 198 ppm), and bound to hemoglobin via van der Waals forces in the red blood cells (RBC, 217 ppm). Measuring the signal uptake dynamics or the ratio of signal in the three compartments (RBC:M, RBC:GAS, or M:GAS) with a simple spectroscopic sequence,[8,9] more advanced modeling with chemical shift saturation recovery experiments[10–12] or with frequency-encoded imaging sequences[4,13,14] provides a direct, quantitative, and in some cases spatially resolved direct measurement of gas uptake in the lungs. Clinical applications of HP ^{129}Xe MR range from quantification of chronic obstructive pulmonary disease[15,16] and asthma[15,17] to interstitial lung diseases,[14,18] and it was recently hypothesized that distinct ^{129}Xe MRI signatures are associated with different cardiopulmonary diseases.[19]

Imaging dissolved-phase xenon is enabled by rapid diffusive uptake in tissues and the long gas phase T_1 (~20 s) of the signal in the alveolar reservoir, but is challenging due to short T_2^* (in the lung: ~2 ms at 1.5 T or ~1 ms at 3 T) and low signal intensity (1%–2% of the gas phase signal). Methods to spatially and spectrally resolve the ^{129}Xe resonances tested in humans include 3D radial 1-point Dixon,[13] 2D CSI,[20] and 3D radial spectroscopic imaging.[14] However, these imaging methods rely on underlying assumptions such as neglecting gas-phase signal contamination and instantaneous acquisition of the data for the 1-point Dixon technique, both of which can introduce non-negligible error in practice. While correction schemes can be applied,[21] it remains that the intensity of the three main frequency components are measured at the expense of discarding rich spectral information. For example, it was demonstrated using global NMR spectroscopy that the frequency shift of the RBC peak was sensitive to blood oxygenation level,[22] and that the M, RBC chemical shift, and the T_2^* relaxation time of the RBC peak were significantly different between healthy volunteers and subjects with idiopathic pulmonary fibrosis.[14,23] Precise maps of chemical shift in addition to transverse relaxation times could therefore be beneficial to directly measure blood oxygenation and related local field inhomogeneity regionally. To our knowledge, only Kammerman et al.[24] have been able to measure simultaneous maps of intensity, transverse relaxation time, and chemical shift via the implementation of a multiple-TE sequence and an iterative modeling of the signal decay, similar to IDEAL reconstruction methods,[25] and their results suggested that the RBC lung T_2^* could be a biomarker of lung injury for the idiopathic pulmonary fibrosis disease.

Applications of dissolved xenon imaging are, however, not limited to the lung, and although other organs are even more challenging due to the lower detectable signals, dissolved xenon MRI has been applied successfully in the kidney[26] and the brain,[27] where results showed up to five dissolved xenon resonances. Standard MRS, spoiled gradient-recalled, and balanced SSFP imaging sequences have been tested for kidney imaging with the goal to measure perfusion as an alternative to arterial spin labeling. For the brain, using HP ^{129}Xe has the advantage of being an injection-free means of imaging the perfusion of cerebral tissue and shows uptake of xenon to the extravascular tissue compartment across the intact blood–brain barrier, with images generally being weighted toward uptake of xenon by gray matter. Recently, the feasibility of using HP ^{129}Xe for clinical applications such as stroke,[28] Alzheimer's disease,[29] and functional MRI[30] has been reported. Dissolved ^{129}Xe in the head exhibits unique chemical shifts for various biochemical compartments that can enable the estimation of gas transfer rates between the compartments,[31] thus potentially providing additional physiological information. Most spectroscopic studies have used whole-brain spectroscopy or full-plane projection for CSI,[27,32] and most MRI methods using conventional frequency and phase encoding have used a thick slice of 50 mm or more.[28–30] Thus, a key aspect limiting the research and development of a wide range of MR methods for HP ^{129}Xe dissolved in the brain is low image resolution.

In both lung and brain imaging with HP ^{129}Xe, increasing the spatial resolution of spectroscopic information would enable regional quantification of MR parameters related to oxygenation and gas exchange. CSI sequences have been used previously, but have hitherto been disregarded for imaging due to associated long acquisition time and reduced image resolution. On the other hand, spectroscopic imaging sequences have been developed and optimized for different multinuclear spectroscopy with similar SNR constraints, such as for ^{13}C or ^{31}P

applications. Greiser et al., for example, developed an efficient density-weighted MRSI technique to tackle the challenges of low SNR, reduced matrix size, and extended FOV by varying the sampling density of phase encoding in k-space.[33] It was validated with in vivo ^{31}P images of the heart, demonstrating an improved shape of the spatial response function and a reduced aliasing artifact due to the small FOV used when compared with uniform sampling. The purpose of this study was to implement the 3D density-weighted MRSI technique for dissolved xenon imaging in the lung and the brain, therefore obtaining spectral information while achieving higher or similar image resolution than the currently used imaging techniques. The method was tested in healthy volunteers at field strengths of 1.5 T and 3 T with the implementation of a spectrally tailored RF pulse for dissolved-phase imaging.

2 | METHODS

2.1 | MRSI acquisition

The density-weighted phase-encoding k-space sampling scheme developed by Greiser et al.[33] was implemented in *MATLAB* (MathWorks, Natick, MA, USA) and used to generate two different 3D spherical sampling patterns. The first one was optimized for lung spectroscopic imaging with a FOV of $30\times30\times15\,cm^3$, targeted matrix size of $14\times14\times7$, 20-kHz bandwidth, and 88 sampling points in the spectral dimension, using 1799 excitations. The k-space sampling distribution is shown in Figure 1 together with its corresponding density compensation function. An optimized crusher gradient and RF spoiling scheme with TR = 8 ms resulted in a total acquisition time of 14.4 s, suitable for a single breath-hold. The second sampling pattern, tailored to brain imaging, consisted of 1101 encoding steps (Figure S1), 288 sampling points, 10-kHz bandwidth, targeted $10\times10\times10$ matrix size, and an isotropic FOV of 18 cm and a TR of 31.2 ms, corresponding to a 34.4-s scan duration. For lung imaging, a spectrally tailored RF pulse with a duration of 1.2 ms and partial self-refocusing was designed for scanning at 1.5 T to excite the dissolved and gas phase with flip angles of 10° and 0.1°, and passbands of 500 Hz and 200 Hz, respectively. The RF pulse shape and frequency distribution can be seen in Figure 2. The same RF pulse shape was also implemented at 3 T after reducing its pulse width by a factor of 2 to 0.6 ms. For brain imaging, a simpler rectangular non–spatially selective RF pulse of 144 μs that offered partial suppression of any remaining gas signal leaking in from the air cavity in the mouth was implemented.

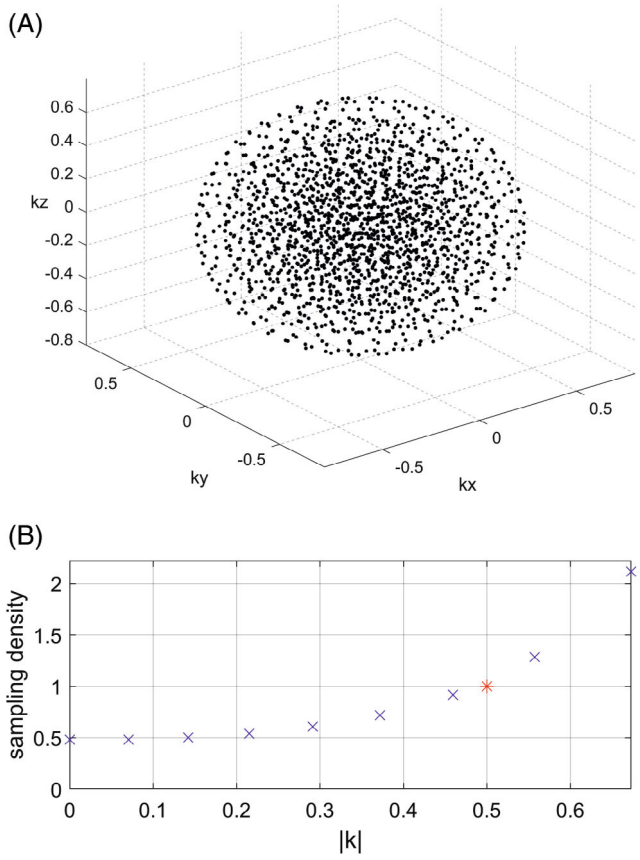

FIGURE 1 A,B, Three-dimensional radial k-space sampling matrix (1799 phase-encoding steps) of the density-weighted spectroscopic imaging used for hyperpolarized (HP) ^{129}Xe lung MRI (A) and the corresponding sampling density as a function of normalized k-space position (B). The red star represents a density of 1 at the k-space location corresponding to the targeted resolution

Brain MRSI was performed on a multinuclear 1.5T GE HDx scanner with a home-built 4-channel receiver RF coil.[34] Lung imaging was performed with a quadrature flexible transmit-receive ^{129}Xe vest RF coil (CMRS, Brookfield, WI, USA) on the same scanner, and 1 volunteer was scanned at 3 T on a GE SIGNA PET/MR scanner. The enriched ^{129}Xe gas was hyperpolarized to an approximate 30% polarization using a regulatory approved spin exchange optical pumping polarizer (POLARIS, Sheffield, UK).[1] One-liter doses of pure xenon (86% enriched ^{129}Xe) were used for all experiments, and imaging was performed during breath-hold. For brain spectroscopic imaging, the start of the sequence was delayed by 4 s to allow dissolved xenon to reach the brain from the lungs via the systemic circulation. Due to the duration of the sequence, the volunteers were instructed to breathe normally 20 s after the start of the breath-hold. Two healthy male volunteers (ages 37 and 38 years) underwent brain imaging, and 4 additional males (ages 30, 31, 35, and 38 years) volunteered for lung imaging at 1.5 T and 1 also at 3 T. All imaging

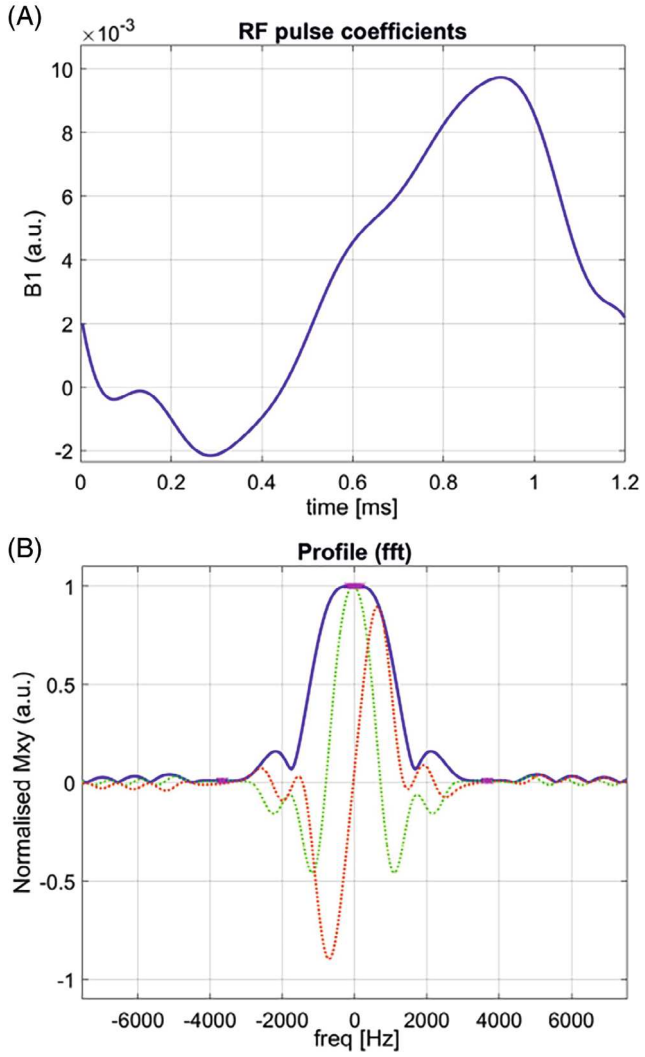

FIGURE 2 A,B, Amplitude envelope of the frequency-tailored RF pulse used for lung imaging at 1.5 T (A) and the frequency response (B). The RF pulse was 1.2 ms long with an isodelay (or time from the peak to the end of the RF excitation pulse) of 0.3 ms and designed to provide 10/0.1° flip angle on the dissolved and gas phase frequencies, respectively

protocols were performed under the approval of the UK National Research Ethics Committee.

2.2 | Data analysis

Data were reconstructed via slow spatial Fourier transformation (i.e., matrix multiplications) directly to a Cartesian grid of $28 \times 28 \times 14$ for lung MRSI and 32^3 for brain MRSI data, respectively, obviating gridding of non-Cartesian k-space locations. The spectral dimension was zero-filled to 256/512 samples for lung/brain data and reconstructed via fast Fourier transformation. Due to the clear separation of the gas, M, and RBC xenon resonances in the lung, a triple Lorentzian automatic fitting routine similar to the method published in Kaushik et al.[35] was implemented in the analysis of the frequency spectrum of each pixel of the lung spectroscopic data, to derive not only the amplitude signal of each component but also its frequency and FWHM/ T_2^* (see Figure 3). After correcting for differences in excitation flip angle between the gas and dissolved resonant frequencies, the RBC:M, RBC:GAS, and M:GAS fractional maps were generated along with T_2^* decay maps and maps of frequency shifts using the gas resonance as the reference. SNR was also calculated as the maximum peak height of each component divided by the RMS of the noise. The noise was measured as the RMS of the real values of

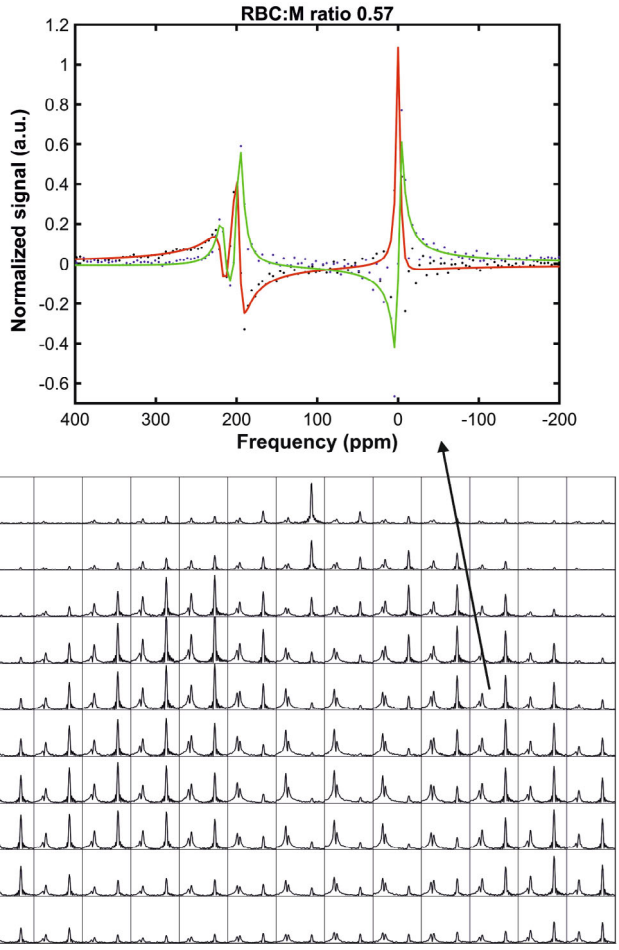

FIGURE 3 Example ^{129}Xe 3D MRSI results in the lung of 1 healthy volunteer at 1.5 T. Top: The data-analysis process for one of the unphased spectra via a triple Lorentzian fitting of the real and imaginary components. Bottom: A montage of the spectra in one coronal slice. The data were reconstructed to the original acquired resolution of $14 \times 14 \times 7$, and a zoom was applied in the frequency and spatial domains in this figure for clarity. In this slice, the trachea can be seen at the top, where a prominent gas peak is clearly visible in the corresponding spectra. For the pixels covering the heart, the RBC peak represents the main component

the spectra outside the lung areas and at frequencies far from the three main xenon resonance frequencies. Masks of the thoracic lung cavity excluding the trachea and the heart were drawn as the region of interest to report mean and SD of the imaging-output parameters. For brain spectroscopic imaging data, the different visible resonances of dissolved xenon reported previously[27] were not sufficiently spectrally resolved with the spectral sampling used here, and a simple integration of the peak areas corresponding primarily to dissolved xenon in the gray matter was therefore used to generate images in all three planes.

3 | RESULTS

3.1 | Lung MRSI

Three-dimensional density-weighted MRSI in combination with the frequency-tailored RF pulse yields spectra in the lungs with sufficient SNR to enable extraction of gas, tissue, and blood maps with robust three-peak Lorentzian fits. Example spectra from the CSI data and results of the triple Lorentzian fitting routine are shown in Figure 3 and Figure S2 for 2 volunteers at 1.5 T and 3 T. Average SNRs of 70, 40, and 19 across the 4 subjects were found for the xenon GAS, M and RBC peaks, respectively (Table 1). Representative signal-amplitude images of the different ^{129}Xe frequency resonances are shown in Figure 4 for a subject at 1.5 T, together with the corresponding ratio maps of signal amplitude (after being corrected for differences in flip angle between dissolved and gas RF excitation) and maps of RBC frequency shift. Similar maps and results obtained at 3 T are illustrated in Figure 5. As can be seen at both field strengths, images are of good quality with lung boundaries distinctly defined and with minimal signal contamination outside the lung, despite the coarse targeted acquisition matrix size of $14 \times 14 \times 7$, demonstrating an appropriate shape of the spatial response from the density-weighted encoding scheme. In the images of all 4 volunteers, the dissolved xenon signal was clearly visible in the left chambers of the heart, especially from the RBC component, due to the absence of any preliminary dummy RF saturation pulses at the start of the sequence and the accumulation of dissolved xenon in the pulmonary vasculature that supply the left heart. This extended contribution from xenon dissolved in the pulmonary veins downstream of the alveolar capillary gas exchange surface could also in part explain the high signal amplitude ratios reported in Table 1, with average RBC:M, RBC:GAS, and M:GAS values of 0.68, 0.0086 and 0.0123, respectively, across the 3 volunteers at 1.5 T.

The M and RBC frequency chemical shifts from the gas resonance are also reported in Table 1. Global values of approximately 198.5 and 215.9 ppm, respectively, and a span of about 0.5 ppm within the lungs were expected for healthy volunteers at 1.5 T and are in line with previously reported publications.[14,35] T_2^* values of approximately 1.8 and 1.5 ms were also measured via the Lorentzian data fitting for dissolved xenon in lung M and RBC, which is shorter than the reported global spectroscopic values in the aforementioned publications at 1.5 T. Differences of T_2^* values between imaging and whole-lung spectroscopy have been previously reported while using a 4-TE image-acquisition strategy and an iterative signal-based model reconstruction.[24] However, the T_2^* values reported here are higher than the global spectroscopic values reported in this latter work. The T_2^* relaxation time was shorter at 3 T, as expected at this field strength,[36]

TABLE 1 Lung imaging results in the 4 healthy volunteers

Subject	1 (1.5 T)	2 (1.5 T)	3 (1.5 T)	4 (3 T)
RBC:M	0.63 ± 0.18	0.75 ± 0.17	0.67 ± 0.15	0.45 ± 0.10
RBC:GAS	0.0086 ± 0.0042	0.0090 ± 0.0061	0.0083 ± 0.0051	0.0050 ± 0.0028
M:GAS	0.0134 ± 0.0030	0.0116 ± 0.0043	0.0121 ± 0.0041	0.0108 ± 0.0030
T_{2M}^*	1.78 ± 0.06 ms	1.79 ± 0.06 ms	1.91 ± 0.11 ms	1.13 ± 0.08 ms
T_{2RBC}^*	1.52 ± 0.08 ms	1.47 ± 0.06 ms	1.5 ± 0.17 ms	1.08 ± 0.12 ms
M chemical shift in ppm	199.0 ± 0.3	198.7 ± 0.3	197.9 ± 0.4	197.8 ± 0.4
RBC chemical shift in ppm	215.9 ± 0.6	216.0 ± 0.5	215.7 ± 1.2	218.3 ± 0.7
SNR GAS	72 ± 26	100 ± 47	64 ± 27	76 ± 28
SNR M	46 ± 20	50 ± 22	36 ± 13	28 ± 11
SNR RBC	21 ± 9	28 ± 12	16 ± 7	11 ± 4

Note: Values are displayed as mean ± SD over a lung region of interest excluding the heart and the trachea. T_2^* values were calculated as the inverse of Pi times the FWHM derived from the fitting routine. The SNR was calculated as the maximum absolute peak value divided by the noise RMS.

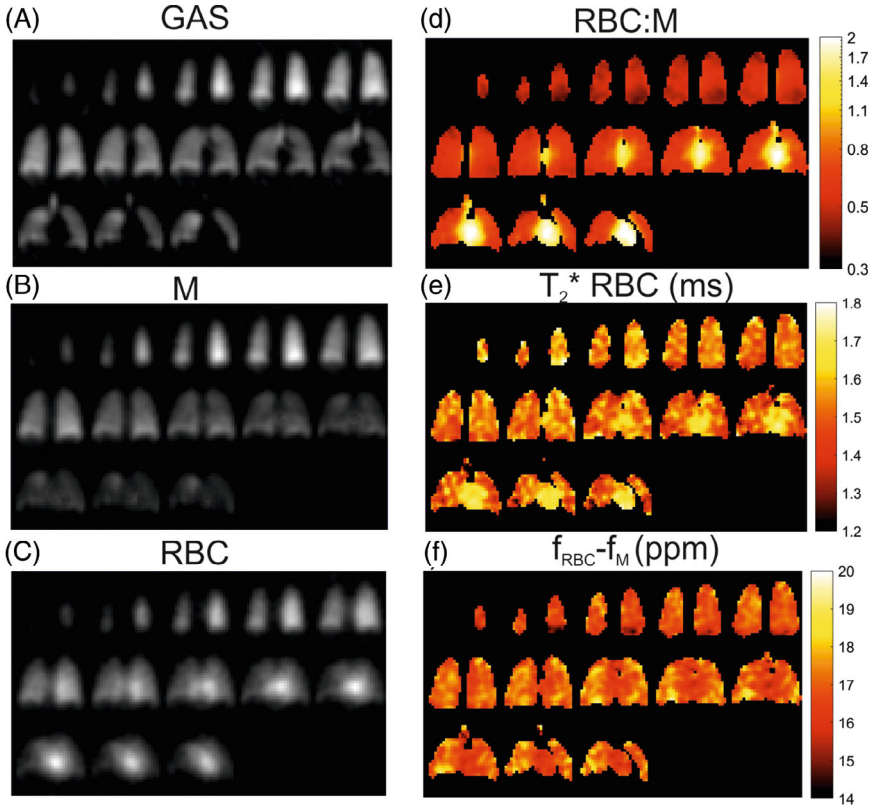

FIGURE 4 The 3D MRSI of the lung of a healthy volunteer at 1.5 T. A, ventilation image. B, Membrane (M) image. C, Red blood cells (RBC) image. D, RBC:M ratio map. E, T_2^* RBC map. F, RBC frequency shift map (in ppm from M reference)

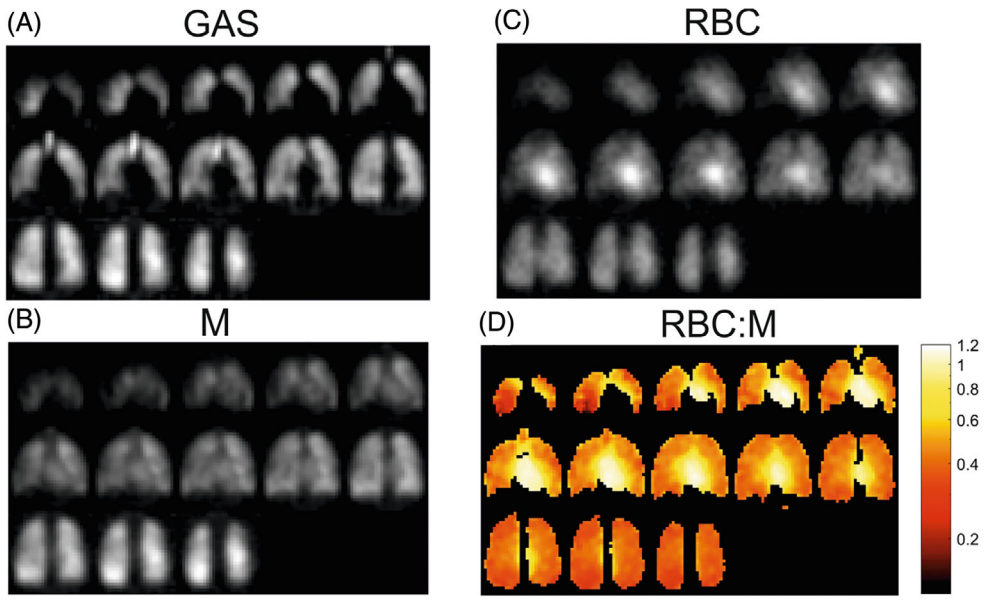

FIGURE 5 The 3D MRSI of the lung of a healthy volunteer at 3 T. A, Ventilation image. B, Membrane image. C, RBC image. D, RBC:M ratio map

with average values of 1.13 and 1.08 ms obtained for the healthy volunteer scanned.

3.2 | Brain MRSI

Images of dissolved xenon resonance peaks corresponding to the gray matter are displayed for the 2 healthy volunteers' brain MRSI in Figure 6 with SNR values of 21 ± 5 (mean $\pm$ SD) and 20 ± 6 for the 2 volunteers. The contrast between white and gray matter is clearly visible, and to our knowledge this is the first time that 3D imaging of dissolved xenon in the human brain at the resolution of 2-cm isotropic voxel size has been reported. Although images within the region of interest are of good quality, it is worth noting that signal outside the brain was present for one of the volunteers (Figure 6B), in whom the gas signal was visible in the oral cavity for both volunteers but images are not shown here. The SNR for the xenon in the blood was too low to display corresponding images, as only the locations of the carotid artery could be clearly

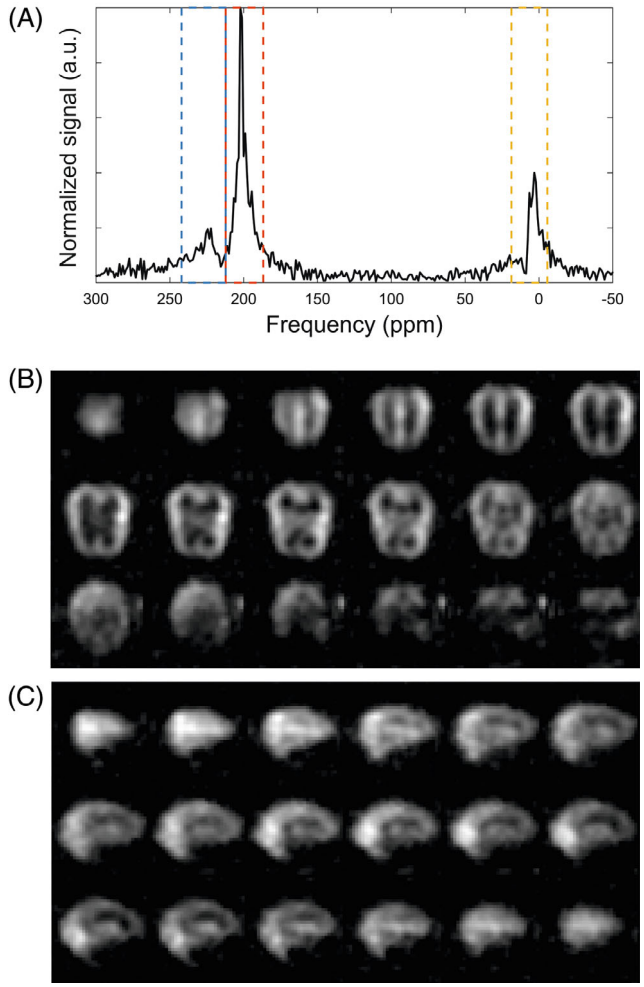

FIGURE 6 The 3D-MRSI results of ^{129}Xe in the brain of 2 healthy volunteers. A, A single spectrum for volunteer 1 showing the different resonances of xenon in the head. The vertical dashed lines represent the limits for integration of the absolute signal of the three main components: gas from the oral cavity at 0 ppm, multiple peaks but mostly weighted by gray matter at approximately 196 ppm and blood at 220 ppm. B, Axial images of the gray-matter peak for volunteer 1. C, Sagittal images for Volunteer 2. Images were reconstructed to a 0.625-cm isotropic resolution

visualized. The frequency shift of the gray matter peak was about 196 ppm apart from the gas reference peak, in line with previously published results.[27]

4 | DISCUSSION

An efficient sampling strategy for 3D MRSI of dissolved HP ^{129}Xe in the human brain and lungs has been demonstrated and validated in healthy volunteers. Results showed that SNR was high enough to obtain good-quality images of the dissolved xenon in the membrane and pulmonary vasculature of the lung as well as good-resolution images of xenon in the gray matter of the brain. With an acquired isotropic resolution of 2 cm, the previously reported slice thickness of 5 cm has been improved by a factor of 2.5,[34] enabling 3D imaging of the brain to be performed. This addresses the main limitation of our previous 2D Cartesian spoiled gradient-recalled technique for clinical translation of HP ^{129}Xe in the brain.[28] While the implementation of an efficient 3D k-space density-weighted CSI[33] is partially responsible for the increase in SNR/decrease in achievable CSI slice thickness, we acknowledge that a significant factor contributing to the improvement when compared with previous 2D-CSI results[27] is the implementation of our four-channel RF coil described in Rao et al.[34] Furthermore, the choice of achieving higher-resolution images of dissolved xenon in the brain has been made at the expense of spectral resolution and displaying solely gray-matter uptake images. Although SNR, spatial, and frequency resolutions are interdependent and subject to the application, the slice thickness could be increased to achieve a better spectral resolution of the xenon peaks in the brain.

For lung imaging, the achieved resolution is comparable to the multi-TE 3D radial spectroscopic imaging published in Collier et al.[14] and Qing et al.[4] while using a similar acquisition time and obtaining additional spectral information for each voxel. Studies with 1-point Dixon imaging techniques currently report acquiring higher image resolution of approximately 0.7–1.25 cm^3,[13,36] although it is far from being the real image resolution, as a kernel sharpness of 0.14 is used during the image reconstruction, which considerably reduces the weighting of the acquired high spatial frequencies.[37,38] It is worth noting that the acquired resolution is the true image resolution presented in this work.

With a density-weighted phase-encoding strategy, the shape of the spatial response function is improved, and higher SNR was achieved when compared to standard Cartesian CSI with apodization. However, this is at the expense of k-space efficiency, as it requires more phase encodes than with a Cartesian sampling strategy. In general, the short T_2^* of dissolved-phase xenon of approximately 1.8 ms (at 1.5 T) in the lung is not favorable to the use of long readout gradients, and it makes a full MRSI strategy similarly RF encoding–efficient as other techniques. Acquiring the full spectrum improves separation of signals, robustness, and confidence in the results. Lung MRSI was successfully implemented at 3 T, a common field strength of choice for scanners with multinuclear capability. Brain MRSI was not tested at 3 T here but is planned in further work.

The RF pulse design for lung MRSI worked robustly and yielded the expected excitation level on the ^{129}Xe gas resonance. The RF pulse was tested before its implementation for MRSI in vitro with a proton phantom and with a bag of HP ^{129}Xe gas, where results showed a reliable 1%

excitation within the pass-bands at 3.5 kHz (7 kHz at 3 T) off resonance. Other groups have previously tried to suppress the gas signal completely from the dissolved xenon data, either because it would be incompatible with the choice of the imaging technique (e.g., 1-point Dixon) or because the gas signal was chosen to be acquired reliably in an RF-excitation interleaved fashion.[4,14] However, inconsistent results have been obtained due to potential nonlinearity of the power response of the RF transmit chain seen on most MRI systems.[39,40] Furthermore, additional correction to remove gas contamination from the signal is necessary.[21] As suggested by our results, we believe that it is much easier to excite the gas phase with a small but defined flip angle than to try to completely suppress it. Moreover, exciting gas signal with a known 0.1° flip angle could offer the advantage of having a reliable gas signal from which quantitative fractional ventilation maps can be derived in the lungs, obviating the need for a separate gas-phase data acquisition, and therefore increasing the number of radial projections and scan-time efficiency.

Regarding the clinical application of MRSI for imaging lung gas transfer with HP ^{129}Xe, a recent effort from the HP ^{129}Xe MRI community resulted in the publication of a standardized protocol,[41] recommending the use of 15-ms TR and 20° flip angle to be able to compare imaging ratios among different centers for multisite clinical trials. Due to the processes of gas exchange and blood transport by the pulmonary circulation, the dissolved xenon signal in the lung is highly dependent on these two imaging parameters. It could therefore be desirable to use these parameters and to add some dummy scans at the start of the sequence, to suppress any prior build-up of xenon magnetization in the pulmonary venous system downstream from the alveolar capillary bed before imaging. However, using a 15-ms TR for the MRSI sequence parameters used here would not be practical, as it would increase the scan time to 27 s for the same sampling pattern, rendering it an inefficient scanning strategy. Ruppert et al.[42] published a flip angle–TR equivalence formula that aims to facilitate standardization of dissolved-phase xenon imaging results. More recently, the same signal model was applied in humans to reduce the scan time of the 1-point Dixon imaging sequence by using the equivalent flip angle/TR parameters of 12° and 5.4 ms.[43] Following this principle and model, the imaging ratios from the MRSI sequence could be directly comparable with most of the published data in the literature by just increasing the flip angle from 10° to 14.6°, adding some dummy scans at higher flip angle at the start of the sequence and keeping the same TR of 8 ms, which can be easily implemented. In the present work, dummy saturation pulses were not implemented in order to maximize SNR and to be able to visualize the dissolved xenon in the blood post capillary and in the heart as a means to further validate the spatial precision of the technique. We expect that, once the dummy scans are implemented, the SNR of dissolved xenon images would drop by about 15%–20% for both lung and brain imaging.

The main limitation of this work was the small validation cohort of healthy volunteers for whom the imaging technique was tested. After implementing the dummy scans and the flip angle/TR parameters equivalence, it would be desirable to acquire data in a large enough cohort to be able to compare our imaging ratios with alternative dissolved-phase imaging techniques. Work is now underway. In addition to the healthy volunteers scanned in this proof-of-principle study, it would also be interesting to test the sensitivity of MRSI with subjects showing abnormally low gas transfer in the lungs (e.g., subjects with interstitial lung diseases or long coronavirus disease symptoms) or reduced brain perfusion (e.g., following stroke). Although it is not possible with this method to measure the amplitude of the ^{129}Xe RBC signal oscillation, as in the case of multi-echo radial spectroscopic imaging,[14] the possibility with this work to assess spectral information for each voxel while achieving a reasonable resolution makes this technique particularly interesting for measuring regional oxygenation in the lung via RBC frequency shift[22] or ^{129}Xe transverse relaxation rates that have been proposed as a biomarker of lung injury.[24] Future work for the brain will focus not only on implementing more complex one-dimensional NMR lineshape fitting routines to assess the different peaks of dissolved xenon regionally in various biochemical compartments in the brain, but also to evaluate whether further improvement in spectral resolution and/or SNR can be obtained at 3 T. Future studies in the lung will aim at benchmarking 1-point/multipoint Dixon types sequences against density-weighted MRSI and compare the results in a group of patients.

5 | CONCLUSIONS

Density-weighted MRSI in combination with frequency-tailored RF excitation is a robust and SNR-efficient approach for detecting xenon gas dissolved in lung tissue and blood with higher spectral resolution than achieved with echo-planar (Dixon/IDEAL) methods. Ratio maps obtained with MRSI could be used to compare results with these imaging techniques and validate the correctness of their underlying assumptions. Two-centimeter isotropic imaging of ^{129}Xe in the brain has also been demonstrated in this work.

ACKNOWLEDGMENT

Medical Research Council: Grant/Award No. MR/M00 8894/1

ORCID

Guilhem J. Collier https://orcid.org/0000-0002-1874-4775
Madhwesha Rao https://orcid.org/0000-0002-4109-4176
Graham Norquay https://orcid.org/0000-0002-4108-9035

REFERENCES

1. Norquay G, Collier GJ, Rao M, Stewart NJ, Wild JM. 129Xe-Rb spin-exchange optical pumping with high photon efficiency. *Phys Rev Lett.* 2018;121:153201.
2. Hersman FW, Ruset IC, Ketel S, et al. Large production system for hyperpolarized 129Xe for human lung imaging studies. *Acad Radiol.* 2008;15:683-692.
3. Birchall JR, Irwin RK, Nikolaou P, et al. XeUS: a second-generation automated open-source batch-mode clinical-scale hyperpolarizer. *J Magn Reson.* 2020;319:106813.
4. Qing K, Ruppert K, Jiang Y, et al. Regional mapping of gas uptake by blood and tissue in the human lung using hyperpolarized xenon-129 MRI. *J Magn Reson Imaging.* 2014;39:346-359.
5. Li H, Zhao X, Wang Y, et al. Damaged lung gas exchange function of discharged COVID-19 patients detected by hyperpolarized (129) Xe MRI. *Sci Adv.* 2021;7:eabc8180.
6. Grist JT, Chen M, Collier GJ, et al. Hyperpolarized (129) Xe MRI abnormalities in dyspneic participants 3 months after COVID-19 pneumonia: preliminary results. *Radiology.* 2021;210033:E353-E360.
7. Albert MS, Kacher DF, Balamore D, Venkatesh AK, Jolesz FA. T(1) of (129) Xe in blood and the role of oxygenation. *J Magn Reson.* 1999;140:264-273.
8. Weatherley ND, Stewart NJ, Chan HF, et al. Hyperpolarised xenon magnetic resonance spectroscopy for the longitudinal assessment of changes in gas diffusion in IPF. *Thorax.* 2019;74:500-502.
9. Bier EA, Robertson SH, Schrank GM, et al. A protocol for quantifying cardiogenic oscillations in dynamic (129) Xe gas exchange spectroscopy: the effects of idiopathic pulmonary fibrosis. *NMR Biomed.* 2019;32:e4029.
10. Stewart NJ, Leung G, Norquay G, et al. Experimental validation of the hyperpolarized (129) Xe chemical shift saturation recovery technique in healthy volunteers and subjects with interstitial lung disease. *Magn Reson Med.* 2015;74:196-207.
11. Patz S, Muradyan I, Hrovat MI, et al. Diffusion of hyperpolarized Xe-129 in the lung: a simplified model of Xe-129 septal uptake and experimental results. *New J Phys.* 2011;13:015009.
12. Chang YV, Quirk JD, Ruset IC, Atkinson JJ, Hersman FW, Woods JC. Quantification of human lung structure and physiology using hyperpolarized ^{129}Xe. *Magn Reson Med.* 2014;71:339-344.
13. Kaushik SS, Robertson SH, Freeman MS, et al. Single-breath clinical imaging of hyperpolarized (129) Xe in the airspaces, barrier, and red blood cells using an interleaved 3D radial 1-point Dixon acquisition. *Magn Reson Med.* 2016;75:1434-1443.
14. Collier GJ, Eaden JA, Hughes PJC, et al. Dissolved (129) Xe lung MRI with four-echo 3D radial spectroscopic imaging: quantification of regional gas transfer in idiopathic pulmonary fibrosis. *Magn Reson Med.* 2021;85:2622-2633.
15. Qing K, Mugler JP 3rd, Altes TA, et al. Assessment of lung function in asthma and COPD using hyperpolarized 129Xe chemical shift saturation recovery spectroscopy and dissolved-phase MRI. *NMR Biomed.* 2014;27:1490-1501.
16. Ruppert K, Qing K, Patrie JT, Altes TA, Mugler JP 3rd. Using hyperpolarized Xenon-129 MRI to quantify early-stage lung disease in smokers. *Acad Radiol.* 2019;26:355-366.
17. Mugler JP 3rd, Altes TA, Ruset IC, et al. Simultaneous magnetic resonance imaging of ventilation distribution and gas uptake in the human lung using hyperpolarized xenon-129. *Proc Natl Acad Sci U S A.* 2010;107:21707-21712.
18. Wang Z, Robertson SH, Wang J, et al. Quantitative analysis of hyperpolarized (129) Xe gas transfer MRI. *Med Phys.* 2017;44:2415-2428.
19. Wang Z, Bier EA, Swaminathan A, et al. Diverse cardiopulmonary diseases are associated with distinct xenon magnetic resonance imaging signatures. *Eur Respir J.* 2019;54:1900831.
20. Doganay O, Chen M, Matin T, et al. Magnetic resonance imaging of the time course of hyperpolarized (129) Xe gas exchange in the human lungs and heart. *Eur Radiol.* 2019;29:2283-2292.
21. Hahn AD, Kammerman J, Fain SB. Removal of hyperpolarized (129) Xe gas-phase contamination in spectroscopic imaging of the lungs. *Magn Reson Med.* 2018;80:2586-2597.
22. Norquay G, Leung G, Stewart NJ, Wolber J, Wild JM. (129) Xe chemical shift in human blood and pulmonary blood oxygenation measurement in humans using hyperpolarized (129) Xe NMR. *Magn Reson Med.* 2017;77:1399-1408.
23. Robertson SH, Virgincar RS, Bier EA, et al. Uncovering a third dissolved-phase (129) Xe resonance in the human lung: quantifying spectroscopic features in healthy subjects and patients with idiopathic pulmonary fibrosis. *Magn Reson Med.* 2017;78:1306-1315.
24. Kammerman J, Hahn AD, Cadman RV, Malkus A, Mummy D, Fain SB. Transverse relaxation rates of pulmonary dissolved-phase hyperpolarized (129) Xe as a biomarker of lung injury in idiopathic pulmonary fibrosis. *Magn Reson Med.* 2020;84:1857-1867.
25. Tsao J, Jiang Y. Hierarchical IDEAL: fast, robust, and multiresolution separation of multiple chemical species from multiple echo times. *Magn Reson Med.* 2013;70:155-159.
26. Chacon-Caldera J, Maunder A, Rao M, et al. Dissolved hyperpolarized xenon-129 MRI in human kidneys. *Magn Reson Med.* 2020;83:262-270.
27. Rao M, Stewart NJ, Norquay G, Griffiths PD, Wild JM. High resolution spectroscopy and chemical shift imaging of hyperpolarized (129) Xe dissolved in the human brain in vivo at 1.5 tesla. *Magn Reson Med.* 2016;75:2227-2234.
28. Rao MR, Norquay G, Stewart NJ, Hoggard N, Griffiths PD, Wild JM. Assessment of brain perfusion using hyperpolarized (129) Xe MRI in a subject with established stroke. *J Magn Reson Imaging.* 2019;50:1002-1004.
29. Hane FT, Li T, Plata JA, Hassan A, Granberg K, Albert MS. Inhaled xenon washout as a biomarker of Alzheimer's disease. *Diagnostics.* 2018;8:41.
30. Shepelytskyi Y, Hane FT, Grynko V, Li T, Hassan A, Albert MS. Hyperpolarized Xe-129 time-of-flight MR imaging of perfusion and brain function. *Diagnostics.* 2020;10:630.
31. Rao MR, Norquay G, Stewart NJ, Wild JM. Measuring Xe-129 transfer across the blood-brain barrier using MR spectroscopy. *Magn Reson Med.* 2021;85:2939-2949.

32. Kilian W, Seifert F, Rinneberg H. Dynamic NMR spectroscopy of hyperpolarized Xe-129 in human brain analyzed by an uptake model. *Magn Reson Med.* 2004;51:843-847.
33. Greiser A, von Kienlin M. Efficient k-space sampling by density-weighted phase-encoding. *Magn Reson Med.* 2003;50:1266-1275.
34. Rao MR, Stewart NJ, Griffiths PD, Norquay G, Wild JM. Imaging human brain perfusion with inhaled hyperpolarized (129) Xe MR imaging. *Radiology.* 2018;286:659-665.
35. Kaushik SS, Freeman MS, Yoon SW, et al. Measuring diffusion limitation with a perfusion-limited gas—hyperpolarized 129Xe gas-transfer spectroscopy in patients with idiopathic pulmonary fibrosis. *J Appl Physiol.* 2014;117:577-585.
36. Wang Z, He M, Bier E, et al. Hyperpolarized (129) Xe gas transfer MRI: the transition from 1.5T to 3T. *Magn Reson Med.* 2018;80:2374-2383.
37. Robertson SH, Virgincar RS, He M, Freeman MS, Kaushik SS, Driehuys B. Optimizing 3D noncartesian gridding reconstruction for hyperpolarized Xe-129 MRI—focus on preclinical applications. *Concept Magn Reson A.* 2015;44:190-202.
38. Pipe JG. Reconstructing MR images from undersampled data: data-weighting considerations. *Magn Reson Med.* 2000;43:867-875.
39. Kaushik SS, Freeman MS, Cleveland ZI, et al. Probing the regional distribution of pulmonary gas exchange through single-breath gas- and dissolved-phase 129Xe MR imaging. *J Appl Physiol.* 2013;115:850-860.
40. Leung G, Norquay G, Schulte RF, Wild JM. Radiofrequency pulse design for the selective excitation of dissolved 129Xe. *Magn Reson Med.* 2015;73:21-30.
41. Niedbalski PJ, Hall CS, Castro M, et al. Protocols for multi-site trials using hyperpolarized (129) Xe MRI for imaging of ventilation, alveolar-airspace size, and gas exchange: a position paper from the (129) Xe MRI clinical trials consortium. *Magn Reson Med.* 2021;86:2966-2986.
42. Ruppert K, Amzajerdian F, Hamedani H, et al. Assessment of flip angle-TR equivalence for standardized dissolved-phase imaging of the lung with hyperpolarized 129Xe MRI. *Magn Reson Med.* 2018;81:1784-1794.
43. Niedbalski PJ, Lu J, Hall CS, et al. Utilizing flip angle/TR equivalence to reduce breath hold duration in hyperpolarized (129) Xe 1-point Dixon gas exchange imaging. *Magn Reson Med.* 2022;87:1490-1499.

SUPPORTING INFORMATION

Additional supporting information may be found in the online version of the article at the publisher's website.

Figure S1. A,B, Three-dimensional radial k-space sampling matrix (1101 phase-encoding steps) of the density-weighted spectroscopic imaging used for hyperpolarized (HP) ^{129}Xe lung MRI (A) and the corresponding sampling density as a function of normalized k-space position (B)

Figure S2. Example ^{129}Xe 3D-MRSI results in the lung of 1 healthy volunteer at 3 T. Top: The data-analysis process for one of the unphased spectra via a triple Lorentzian fitting of the real and imaginary components. Bottom: A montage of the spectra in one coronal slice. The data were reconstructed to the original acquired resolution of $14 \times 14 \times 7$ and a zoom was applied in the frequency and spatial domains in this figure for clarity. In this slice, the trachea can be seen at the top where a prominent gas peak is clearly visible in the corresponding spectra. For the pixels covering the heart, the red blood cell (RBC) peak represents the main component

How to cite this article: Collier GJ, Schulte RF, Rao M, Norquay G, Ball J, Wild JM. Imaging gas-exchange lung function and brain tissue uptake of hyperpolarized ^{129}Xe using sampling density-weighted MRSI. *Magn Reson Med.* 2023;1-10. doi: 10.1002/mrm.29602